Binary-Component Self-Assembled Monolayer Comprising Tetrathiafulvalene and *n*-Tetradecane Molecules with Periodic Ordered Phase Separation Structures on a Highly Oriented Pyrolytic Graphite Surface

Miao Zhao,[†] Ke Deng,[†] Peng Jiang,*[,†] Si-Shen Xie,[‡] Denis Fichou,[§] and Chao Jiang*[,†]

National Center for Nanoscience and Technology (NCNST), Beijing 100190, P. R. China, Institute of Physics, Beijing National Laboratory for Condensed Matter Physics, Chinese Academy of Sciences (CAS), Beijing 100190, P. R. China, and CEA-Saclay, Organic Nanostructures & Semiconductors Laboratory, CNRS-CEA-UPMC, SPCSI, 91191 Gif-sur-Yvette, France

Received: November 11, 2009

A binary-component self-assembled monolayer (SAM) comprising tetrathiafulvalene (TTF) and *n*-tetradecane (*n*-$C_{14}H_{30}$) molecules has been investigated by a scanning tunneling microscope (STM) on a highly oriented pyrolytic graphite (HOPG) surface at room temperature. High-resolution STM images of the SAM reveal that the two different kinds of molecules spontaneously form periodic ordered strip-like phase separation structure on the HOPG substrate. The phenomenon can be qualitatively understood in terms of a phase field model, in which the interplay of three ingredients, including free energy of the binary component solution monolayer, phase boundary energy, and surface stress, is suggested to play an important role in determining the equilibrium sizes of strip-like domains of the TTF and *n*-$C_{14}H_{30}$ in the ordered phase separation structure. In addition, scanning tunneling spectrum (STS) measurements have also been performed by operating an STM tip to locate on the individual TTF or *n*-$C_{14}H_{30}$ molecule in the SAM on the HOPG substrate. The STS at the TTF molecule shows a distinct rectifying behavior, while at the *n*-$C_{14}H_{30}$ molecule it shows an intrinsic small current increase with the change of bias voltage and a slight asymmetry.

1. Introduction

In recent years, fabrication of electronic devices based on organic semiconductor materials has attracted more attention because of their potential applications in low-cost, large-area flexible display electronics.[1,2] In comparison to inorganic materials, organics are easily dissolved in a suitable solvent and then cast over a soft substrate for construction of device units through a simple solution phase process. Structure-dependent intermolecular interactions including hydrophobic forces, $\pi-\pi$, hydrogen bonds and electrostatic forces can spontaneously drive the formation of ordered organic nanostructures on a substrate surface.[3−10] The molecular self-assembly method provides a promising bottom-up route to build functionalized organic molecule arrays for the electronic components with desired electric properties. However, unlike their crystallization in solution that only depends on intermolecular interactions, the crystallized structures of organic molecules on solid surfaces also rely on the surface structure and the properties of the substrate. That is, the existence of the solid interface can significantly influence adsorption strength, molecule conformation, and further structures of the formed organic molecule aggregates.

Tetrathiafulvalene (TTF) and its derivatives (TTFs) exhibit strong electron-donor abilities and have been successfully used as building blocks to form charge transfer salts and organic conductors because of their special structures and rich electron nature.[11−13] TTF molecules have a π-conjugated structure with four sulfur atoms (see Scheme 1). They can crystallize into submicrometer-scaled single crystal belt structures with two kinds of polymorphs, i.e., monoclinic α-TTF and triclinic β-TTF, in solution.[14] For the α phase, TTF molecules arrange themselves along the short *b* axis by intermolecular $\pi-\pi$ stacking and S···S interactions in the manner of a herringbone structure. In contrast, for the β phase, TTF molecules form infinite chains by intermolecular S···S interactions among the closest-neighbor TTF molecules. The crystalline structures of the obtained products rely on the solvent used. For example, α-TTF single crystal belts are formed when using *n*-heptane as a solvent, while β-TTF ones are obtained if using chlorobenzene. This finding provides a convincing example of the effect of the interactions between TTF and solvent molecules on crystallized structures of the TTF molecules in the solution.[15]

De Schryver and De Feyter have initiated systematic studies on the adsorption and assembly behaviors of a series of TTFs at the interface between a layer of solution and a highly oriented

SCHEME 1: A Chemical Structure Model of a TTF Molecule[a]

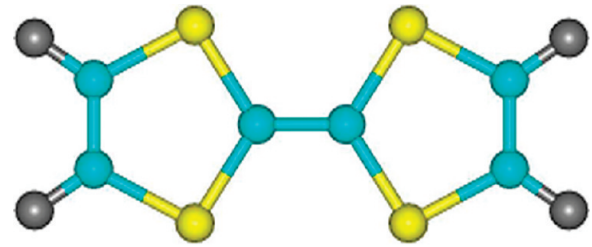

[a] Yellow, blue, and gray are sulfur, carbon, and hydrogen atoms, respectively.

* To whom correspondence should be addressed. E-mail: pjiang@nanoctr.cn (P.J.); jiangch@nanoctr.cn (C.J.). Tel: +86-10-82545549. Fax: +86-10-62656765.
[†] National Center for Nanoscience and Technology.
[‡] Chinese Academy of Sciences.
[§] CEA-Saclay.

10.1021/jp9107427
Published on Web 12/07/2009

pyrolytic graphite (HOPG) surface by a scanning tunneling microscope (STM).[16−19] In their pioneer studies, they observed that TTFs bearing different chemical functional groups such as amides, phenyl rings, or long alkyl chain groups exhibit different assembly patterns on the HOPG surface. These functional groups are designed to improve or tune TTFs nanostructures that are spontaneously formed on the substrate through additional group−group or group−substrate interactions. Furthermore, they have found that the solvent effects also play a role in determining two-dimensional patterns of the TTFs on the HOPG. In this work, we report the self-assembly behavior of the basic TTF molecules by depositing a drop of TTF n-tetradecane (n-$C_{14}H_{30}$) solution on HOPG substrate. We have observed via STM that the TTF and n-$C_{14}H_{30}$ molecules coadsorb and form a periodic ordered strip-like phase separation structure on the HOPG surface at room temperature. The double-lamella structure formed by the TTF molecules on the HOPG is completely different from the molecular arrangement in any two-dimensional crystal plane in α-TTF and β-TTF crystal phase structures. We explain the possible mechanism of formation of the structure in terms of a substrate-mediated phase field model. Moreover, current−voltage ($I-V$) characteristics of the individual TTF and n-$C_{14}H_{30}$ molecule in the phase-separated SAM have also been explored at room temperature.

2. Experimental Details

TTF (+99%) and n-$C_{14}H_{30}$ (+99%) were obtained from Aldrich Chemical Co. and used without further purification. The TTF was first dissolved in n-$C_{14}H_{30}$ to achieve saturation by ultrasonication processing for ∼10 min. Then, a small droplet of the solution was deposited on a freshly cleaved HOPG surface for STM observation. STM (Agilent Technology) imaging was performed with a sharp tip being immersed in the solution at room temperature. Observations were carried out at different values for both positive and negative sample biases. All images were originally obtained in a constant current mode and without further modification and processing. The STM tips were made by mechanically cutting a piece of Pt/Ir wire (80:20, diameter 0.2 mm). Current imaging tunneling spectroscopy (CITS) measurements were performed when the STM molecule images were reproducibly and stably obtained at the liquid/solid interface. The monolayer prepared from the more concentrated alkane solution did not change monolayer composition and structure. Experiments were repeated with different tips and samples to avoid images with artifacts. Typical imaging parameters were set in the range of 0.3−0.5 V for tip bias voltage and 100−300 pA for tunneling current. High-resolution STM images were obtained after STM scanning for several minutes to hours.

3. Results and Discussion

3.1. STM Imaging Phase Separation Structures of TTF/n-$C_{14}H_{30}$ on HOPG. Figure 1a shows a large-scaled STM image of TTF/ n-$C_{14}H_{30}$ monolayer on an atomically flat HOPG substrate. Domain structures with sizes from several tens to several hundreds of nanometers are visible in the STM image. These domains intersect at 60° or arrange in parallel with one another, reflecting symmetry of the graphite substrate underneath. Domain boundaries can be clearly distinguished. Figure 1b presents an STM image of a local region around a domain boundary in the monolayer. It demonstrates apparent ordered strip-like structures in each domain and some disordered regions around the boundaries, implying a highly dynamic feature of the ordered monolayer in the regions of the boundaries due to the reduced stability of the boundary molecules.[20] Despite the dynamic behavior, the ordered structure in the single domain is still stable enough to endure continuous tip scanning under our imaging conditions.

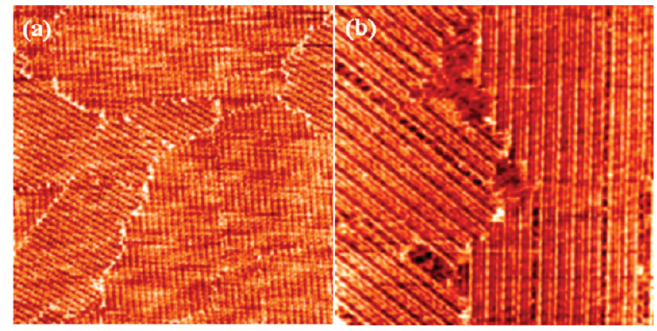

Figure 1. Typical STM images of the mixed ordered monolayer of TTF and n-$C_{14}H_{30}$ molecules on HOPG substrate at various scales: (a) 300 × 300 nm^2 $U_t = -0.4$ V, $I_t = 0.1$ nA; (b) 120 × 120 nm^2 $U_t = -0.6$ V, $I_t = 0.06$ nA.

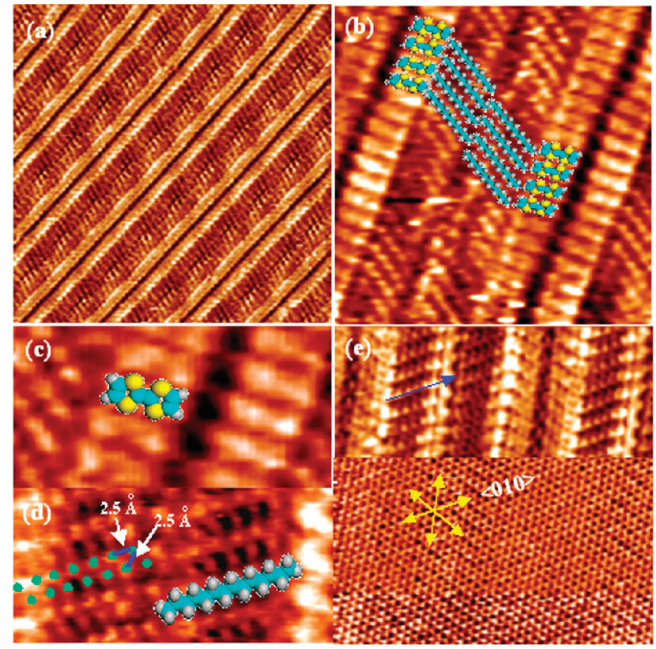

Figure 2. High-resolution STM images of the ordered TTF and n-$C_{14}H_{30}$ molecule ribbon structures with alternate arrangement [(a) 30 × 30 nm^2, $U_t = 0.4$ V, $I_t = 0.1$ nA; (b) 10 × 10 nm^2, $U_t = -0.6$ V, $I_t = 0.1$ nA] showing that the molecules in adjacent different lamella of one ribbon staggeringly arrange with half of the intermolecular spacing in one lamella. Structural modes of TTF and n-$C_{14}H_{30}$ molecules are partly overlaid on the high-resolution STM image [(c) 5 × 2.5 nm^2, $U_t = -0.5$ V, $I_t = 0.1$ nA], in which single TTF molecule and the molecule arrays can be distinguished. A structural mode of a TTF molecule is matched over a protrusion in the STM image [(d) 4.5 × 2.2 nm^2, $U_t = -0.5$ V, $I_t = 0.1$ nA], in which the single n-$C_{14}H_{30}$ molecule is marked by a dashed rectangle, and the hydrogen atoms on various methylene and methyl sites are labeled by 14 green dots. A structural mode of an n-$C_{14}H_{30}$ molecule is matched over a long strip in the STM image [(e) 10 × 10 nm^2, $U_t = -0.6$ V, $I_t = 0.1$ nA], in which the n-$C_{14}H_{30}$-TTF SAM and the HOPG crystal lattice are simultaneously imaged with atom-resolution. Carbon backbones in the n-$C_{14}H_{30}$ molecules are observed to propagate parallel along preferential ⟨010⟩ graphite substrate direction, as indicated by a blue arrow and three yellow ones.

As shown in Figure 2 a−d, high-resolution STM images of the ordered strips demonstrate two kinds of ribbon structures with different widths and bright-dark contrast. The two ribbons periodically alternately arrange. Each kind of ribbon contains

two lamellae with the same size (see Figure 2a,b). The basic building units in the two adjacent lamellae in the same ribbon staggeringly arrange to maximally avoid intermolecular lateral repulsion. For the brighter narrow ribbon, an atomic resolution STM image (see Figure 2c) shows that an individual unit in the lamellae has an average length of 0.83 ± 0.05 nm and a width of 0.30 ± 0.05 nm, being well in accord with the size of a single TTF molecule (ca. 0.81 nm, 0.29 nm). Therefore, we may assign the brighter narrow ribbon to two arrays of the TTF molecules. The average interunit spacing in each array is about 0.28 nm, a little larger than the S−S bond length (0.22 nm) but smaller than the shortest S···S spacing (0.34 nm) in the α-TTF single crystal structure.[21] This suggests that the TTF molecules lie flat on the HOPG surface and form the ordered lamella structure by intermolecular lateral S···S interactions and TTF−graphite $\pi-\pi$ interactions. For the darker wide ribbon, each unit in the ribbon has been measured to have an average length of 1.65 ± 0.05 nm, being in agreement with the length of a single *n*-$C_{14}H_{30}$ molecule (theoretical value 1.64 nm). Thus, we may attribute the wide strip-like structure to two arrays of the *n*-$C_{14}H_{30}$ molecules. In the lamellae, the *n*-$C_{14}H_{30}$ molecules arrange parallel with their long axes. The average distance among the *n*-$C_{14}H_{30}$ molecules is 0.45 ± 0.05 nm, much smaller than the interchain spacing in a three-dimensional alkane crystalline phase (∼0.48 nm). The alkane molecules in neighboring lamellae staggeringly arrange. The angle between the molecular axis and lamella borderline is measured to be ∼60°. Note that no clear interlamellar dark trough can be seen between the two lamellae in the wide ribbon. This suggests that the methyl groups at the alkane-chain ends between two lamellae tend to maximally approach one another. The atomic resolution STM image (see Figure 2d) demonstrates that the basic *n*-$C_{14}H_{30}$ molecule unit in the lamellae is featured by fourteen bright spots with a zigzag array, as marked by a structural mode of a TTF molecule in Figure 2d. The bright spots are separated by an average distance of 2.54 ± 0.05 Å in a row along the direction of the molecule axis and by the nearly same distance of 2.54 ± 0.05 Å between adjacent row spots within a molecule. These bright protrusions can be associated with the sites of topmost hydrogen atoms of the methylene and methyl groups in the single *n*-$C_{14}H_{30}$ molecule since the projecting hydrogen atoms dominate local electron state density.[22−24] This shows that the *n*-$C_{14}H_{30}$ molecular backbone is parallel to the graphite surface in an *all-trans* conformation.

To gain further insight into orientations of the adsorbed *n*-$C_{14}H_{30}$ molecules with respect to the HOPG lattice, we have simultaneously imaged the *n*-$C_{14}H_{30}$/TTF binary component SAM and underlying HOPG lattice in one STM image by modulating STM imaging parameters. Figure 2e shows a STM image of the ordered monolayer at the upper part and HOPG lattice at the lower part. The contrast STM imaging clearly indicates that the *n*-$C_{14}H_{30}$ molecular axis propagates along preferential ⟨010⟩ directions of the graphite substrate. The observation is consistent with the adsorption model of alkane molecules suggested by Groszek.[25] That is, the excellent match of length (0.251 nm) of the C−C−C zigzag chain in the alkane skeleton with the hollow−hollow spacing (0.246 nm) in graphite lattice greatly enhances the commensurate adsorption of the alkane molecules along preferential ⟨010⟩ substrate directions.

As observed in these STM images, TTF molecules can crystallize into an ordered double-lamella structure with alternate *n*-$C_{14}H_{30}$ double-lamella on the HOPG surface. Obviously, the two-dimensional ordered structure of the TTF molecules is completely different from the close-packed herringbone structure in the α-TTF crystal or the chain-like structure in the β-TTF crystal. This shows that the coexistence of the solvent molecules and the HOPG substrate significantly influences the packing density and pattern of the TTF molecules. We can demonstrate in Figure 2b that each TTF molecule corresponds to one *n*-$C_{14}H_{30}$ molecule, i.e., the ratio of TTF versus *n*-$C_{14}H_{30}$ is 1:1 in the SAM with periodic phase separation structures. By carefully considering all feature distances, molecular sizes, dimensions, and geometry, we suggest one possible packing model for the periodic ordered *n*-$C_{14}H_{30}$/TTF SAM on the HOPG (see Figure 3).

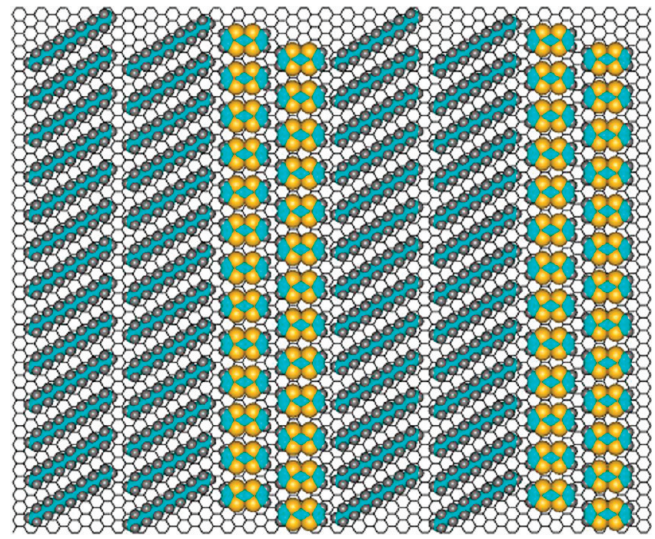

Figure 3. A possible packing pattern of the alternate TTF and *n*-$C_{14}H_{30}$ molecules with lamellar structures on an HOPG substrate.

3.2. A possible Theoretical Explanation of the *n*-$C_{14}H_{30}$/DP-TTF Phase Separation Structures. Phase separation is the transformation of a multicomponent homogeneous system into two or more phases. In our work, the *n*-$C_{14}H_{30}$/TTF solution system exhibits binary phase separation behavior on the HOPG surface. To better understand the substrate-mediated phase separation, we introduce a phase field model[26] to qualitatively explain the observed phenomenon. For simplicity, for the periodic strip-like phase separation structure of the *n*-$C_{14}H_{30}$/TTF monolayer on the substrate, we assume that the free energy of the inner substrate or the bulk remains unchanged. In this case, we can ignore the bulk free energy and only consider the surface free energy. The free energy includes a bicomponent solution monolayer and several layers of the substrate surface beneath the solution monolayer. The surface energy per unit area can be expressed as

$$\Gamma = g(C) + h(C)C_\beta C_\beta + f_{\alpha\beta}(C)\varepsilon_{\alpha\beta} \qquad (1)$$

where Γ, $g(C)$, $h(C)$, and $f_{\alpha\beta}(C)$ are all functions of a component concentration C. In eq 1, $g(C)$ is the free energy of the monolayer solution without the presence of the solid substrate. Assuming that the initial surface monolayer solution is a regular solution, g(C) can be written as

$$g(C) = g_A(1 - C) + g_B C + \Lambda kT[C \ln C + (1 - C)\ln(1 - C) + \Omega C(1 - C)] \qquad (2)$$

in which g_A and g_B are the free energies of pure components A and B, respectively, Λ is the number of molecular positions per unit area on the surface, k is Boltzmann's constant, and T is the absolute temperature. Within the bracket, the first and second terms result from the mixing entropy, and the third one results from the mixing enthalpy. The dimensionless number

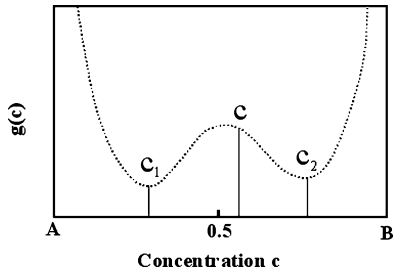

Figure 4. The schematic curve of the free energy double-well function with the concentration C of one of the binary components. $g(C)$ is the surface energy per unit area of a uniform solution monolayer on an unstrained substrate. C is the concentration of one of the binary components.

Ω reflects the difference among the interaction energies including E_{A-A}, E_{B-B}, and E_{A-B} relative to kT. Once introducing a solid surface into the solution system, more energy factors should be considered. In eq 1, the second item, $h(C)C_\beta C_\beta$, represents phase boundary energy, $h(C)$ is a function of the concentration, and the direction of the concentration gradient. C_β is the concentration gradient. The third item in eq 1 $f_{\alpha\beta}$, is called the surface stress tensor, representing the surface energy change associated with per unit elastic strain, and $\varepsilon_{\alpha\beta}$ is the strain in the surface, while α,β represent two different phases.

Now we can come back to qualitatively analyze the observed periodical phase separation structure of the pattern of n-$C_{14}H_{30}$ and TTF molecules on the HOPG substrate. When a droplet of the TTF n-$C_{14}H_{30}$ solution is deposited on the HOPG surface at room temperature, the solution rapidly disperses and covers the whole substrate surface. We assume that the level of concentration on the surface solution achieves uniformity on the HOPG surface at the initial stage. If considering C as the concentration of n-$C_{14}H_{30}$ molecules, for phase separation, $g(C)$ can be expressed as a double-well function (see Figure 4). With the gradual evaporation of the n-$C_{14}H_{30}$ solvent molecules at room temperature, once the concentration C of the solvent molecules in the monolayer solution on the HOPG falls in the zone between C_1 and C_2, phase separation occurs to facilitate the decrease of free energy of the system. When a solid surface exists, the interactions between the substrate and adsorbates must be considered. That is, preferential adsorption of one kind of molecules or coadsorption of both molecules on the substrate may induce the nucleation and growth of the phase made of that molecule. In our case, the length (0.251 nm) of the C−C−C zigzag chains of n-$C_{14}H_{30}$ molecules can match the hollow−hollow spacing (0.246 nm) of the surface graphite lattice much better than FTT molecules do. Thus, the alkane molecules probably adsorb preferentially on the HOPG surface. As a result, a local nonuniform concentration field is induced, which further accelerates a local convective mass transport of the two different components. This process can increase the local concentration of the second component. When the local concentration of the second component achieves a certain value, a new phase for the second component is locally nucleated and grown on the HOPG surface. On one hand, under certain temperature conditions, the appearance of the new phases on the substrate surface creates phase boundaries. If considering the second item in eq 1, the system free energy will increase with the increase of the total phase boundary length. Thus, small domains of the new phase become larger to decrease phase boundary length to release excess boundary energy. On the other hand, the difference of surface stresses in the TTF and n-$C_{14}H_{30}$ phases can lead to an elastic field in the HOPG substrate. On the basis of the third item in eq 1, phase refining will facilitate the decrease of free energy of the system. Therefore, it might be the balance between the phase boundary energy and the nonuniform surface stress that dominates equilibrium sizes of the TTF and the n-$C_{14}H_{30}$ phases. We have also observed that the n-$C_{14}H_{30}$ molecules prefer to orient along ⟨010⟩ directions of the graphite substrate. This suggests that the most compliant orientations adapted by the molecules on the graphite substrate should be those that favor minimal surface stress. The anisotropy of the surface stress breaks the substrate symmetry and causes the ordered stripe-like structures. This in turn influences the arrangement of the TTF lamellae.[27]

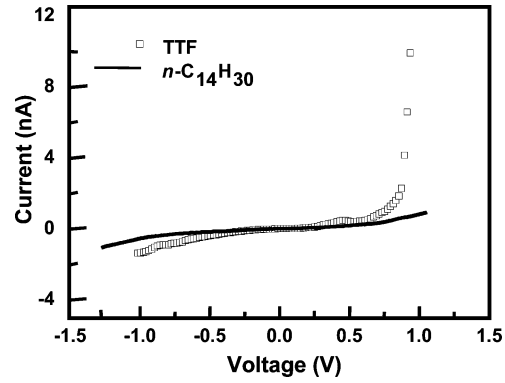

Figure 5. Scanning tunneling spectra ($I-V$ curves) obtained by using an STM tip to address the single TTF (open square) and n-$C_{14}H_{30}$ molecule (black line) at the liquid−graphite interface (the presented curve is averaged over 25 spectra).

3.3. Electron Tunneling Properties of Single DP-TTF and n-$C_{14}H_{30}$ Molecule in the Stripe-Like Structures. To explore electronic properties of single unit in the ordered monolayer structure, CITS measurements were taken to record the tunneling current−voltage ($I-V$) curves at molecule sites in a scanned region. During the detection process, a high-resolution STM image of the ordered TTF/ n-$C_{14}H_{30}$ monolayer was first acquired at selected I_o and V_o. During the second scanning process, at some preset sites in the image, the feedback loop was shut off, and a series of bias voltage was simultaneously applied and the tunneling current was registered. After that, STM imaging parameters were returned to I_o and V_o. The feedback loop was turned on for STM imaging again. Each $I-V$ spectrum at each selected site in the topographic STM image can be obtained in only a few milliseconds. In this case, thermal drift during the process of $I-V$ curve measurements can be induced at the tip-addressed position at room temperature. Figure 5 shows statistical scanning tunneling spectroscopy (STS) collected at the positions of the TTF molecules in the ordered TTF/ n-$C_{14}H_{30}$ monolayer by considering 25 similar spectra. The $I(V)$ curve demonstrates a clear rectifying behavior in which tunneling current rapidly rises above ~0.75 V in the positive applied voltage region. $I(V)$ curves obtained by addressing the tip on the adsorbed single solvent molecules exhibit a small current increase with voltage change and slight asymmetry, implying the intrinsic asymmetry of the tunneling gap. This phenomenon was suggested to be highly associated with the first oxidation potential of the TTF in solution.[28] Casado et al.[29] evaluated the highest energy occupied molecular orbital (HOMO) and lowest energy unoccupied molecular orbital (LUMO) level locations of a series of TTF derivatives as a function of the chemical architecture. The HOMO positions of investigated TTF and derivatives are in the range from −4.6 to −5.1 eV. These values are considerably close to the Fermi level position of graphite (−4.7 eV), which makes electron resonant tunneling possible. A theoretical study on the resonant tunneling reveals

that abrupt current enhancement takes place at a potential position corresponding to the energy level of the oxidized state of the adsorbed molecules.[30] Some experimental investigations also show that orbital-mediated tunneling can induce larger current than that originated from direct electron tunneling.[31,32] However, the molecular rectifying behavior that was observed in this study can not be completely understood in terms of the mechanism because of the larger abrupt change of the tunneling current in the range of positive voltage.[28] The transient configuration of the detecting molecule might also be part of the origin of the phenomenon. Further studies are needed to elucidate the origin of this phenomenon.

4. Conclusion

In conclusion, we have observed the formation of periodic ordered strip-like phase separation structures of TTF and n-$C_{14}H_{30}$ molecules with sharp linear boundaries on an HOPG surface. The finding can be qualitatively understood in terms of a phase field model, in which the interplay of three ingredients, including free energy of binary component solution monolayer, phase boundary energy, and surface stress, determines equilibrium sizes of the TTF and n-$C_{14}H_{30}$ ordered phases. The average STS of the single TTF in the SAM shows a remarkable rectifying behavior in $I(V)$ characteristics, while that of the single n-$C_{14}H_{30}$ molecule only exhibits a small current increase with the voltage change and slight asymmetry.

Acknowledgment. The work was supported by grants from the National Natural Science Foundation of China (No.50772024), the Opening Research Foundation of the National Center for Nanoscience and Technology (NCNST), China, the National Basic Research Program of China (2006CB932600, 2009CB930702, KJCX2-YW-M13), and the "Hundred Talent Program" of the Chinese Academy of Sciences.

References and Notes

(1) Forrest, S. *Nature* **2004**, *428*, 911.
(2) Mas-Torrent, M.; Rovira, C. *Chem. Soc. Rev.* **2008**, *37*, 827.
(3) Dubois, L. H.; Nuzzo, R. G. *Annu. Rev. Phys. Chem.* **1992**, *43*, 437.
(4) Cry, D. M.; Venkataraman, B.; Flynn, G. W. *Chem. Mater.* **1996**, *8*, 1600.
(5) Smith, R. K.; Lewis, P. A.; Weiss, P. S. *Prog. Surf. Sci.* **2004**, *75*, 1.
(6) Gomar-Nadal, E.; Puigmartí-Luis, J.; Amabilino, D. *Chem. Soc. Rev.* **2008**, *37*, 490.
(7) Yang, G.; Liu, G. Y. *J. Phys. Chem. B.* **2003**, *107*, 8746.
(8) De Feyter, S.; Gesquiere, A.; Abdel-Mottaleb, M. M.; Grim, P. C. M.; De Schryver, F. C.; Meiners, C.; Sieffert, M.; Valiyaveettil, S.; Müllen, K. *Acc. Chem. Res.* **2000**, *33*, 520.
(9) Stepanow, S.; Lingenfelder, M.; Dmitriev, A.; Spillmann, H.; Delvigne, E.; Lin, N.; Deng, X.; Cai, C.; Barth, J. V.; Kern, K. *Nat. Mater.* **2004**, *3*, 229.
(10) (a) Katsonis, N.; Marchenko, A.; Fichou, D. *J. Am. Chem. Soc.* **2002**, *124*, 9998. (b) Katsonis, N.; Marchenko, A.; Fichou, D. *J. Am. Chem. Soc.* **2003**, *125*, 13682. (c) Piot, L.; Marchenko, A.; Wu, J. S.; Müllen, K.; Fichou, D. *J. Am. Chem. Soc.* **2005**, *127*, 16245. (d) Jiang, P.; Nion, A.; Marchenko, A.; Piot, L.; Fichou, D. *J. Am. Chem. Soc.* **2006**, *128*, 12390. (e) Nion, A.; Jiang, P.; Popoff, A.; Fichou, D. *J. Am. Chem. Soc.* **2007**, *129*, 2450.
(11) Gorgues, A.; Hudhomme, P.; Salle, M. *Chem. Rev.* **2004**, *104*, 5151.
(12) Bendikov, M.; Wudl, F.; Perepichka, D. *Chem. Rev.* **2004**, *104*, 4891.
(13) Segura, J.; Martin, N. *Angew. Chem., Int. Ed.* **2001**, *40*, 1372.
(14) Jiang, H.; Yang, X.; Cui, Z.; Liu, Y.; Li, H.; Hu, W.; Zhu, D. *Appl. Phys. Lett.* **2007**, *91*, 123505.
(15) Mas-Torrent, M.; Durkut, M.; Hadley, P.; Ribas, X.; Rovira, C. *J. Am. Chem. Soc.* **2004**, *126*, 984.
(16) Gomar-Nadal, E.; Abdel-Mottaleb, M.; Feyter, S.; Veciana, J.; Rovira, C.; Amabilino, D.; Schryver, F. *Chem. Commun.* **2003**, 906.
(17) Abdel-Mottaleb, M.; Gomar-Nadal, E.; Surin, M.; Uji-i, H.; Mamdouh, W.; Veciana, J.; Lemaur, V.; Rovira, C.; Cornil, J.; Lazzaroni, R. *J. Mater. Chem.* **2005**, *15*, 4601.
(18) Puigmarti-Luis, J.; Minoia, A.; Uji-i, H.; Rovira, C.; Cornil, J.; De Feyter, S.; Lazzaroni, R.; Amabilino, D. *J. Am. Chem. Soc.* **2006**, *128*, 12602.
(19) Lei, S.; Puigmartí-Luis, J.; Minoia, A.; Auweraer, M.; Rovira, C.; Lazzaroni, R.; Amabilino, D.; Feyter, S. *Chem. Commun.* **2008**, 703.
(20) McGonigal, G.; Bernhardt, R.; Yeo, Y.; Thomson, D. *J. Vac. Sci. Technol. B* **1991**, *9*, 1107.
(21) Cooper, W. F.; Edmonds, J. W.; Wudl, F.; Coppens, P. *Cryst. Struct. Commun.* **1974**, *3*, 23.
(22) Rabe, J. P.; Buchholz, S. *Science* **1991**, *253*, 424.
(23) Liang, W.; Whangbo, M.; Wawkuschewski, A.; Cantow, H.; Magonov, S. *Adv. Mater.* **1993**, *5*, 817.
(24) Claypool, C.; Faglioni, F.; Goddard III, W.; Gray, H.; Lewis, N.; Marcus, R. *J. Phys. Chem. B* **1997**, *101*, 5978.
(25) Groszek, A. J. *Adsorption at the Gas−Solid and Liquid−Solid Interface*; Elsevier: New York, 1982.
(26) Suo, Z.; Hong, W. *Proc. Natl. Acad. Sci. U.S.A.* **2004**, *101*, 7874.
(27) Lu, W.; Suo, Z. *Phys. Rev. B* **2002**, *65*, 85401.
(28) Abdel-Mottaleb, M.; Gomar-Nadal, E.; De Feyter, S.; Zdanowska, M.; Veciana, J.; Rovira, C.; Amabilino, D.; De Schryver, F. *Nano Lett.* **2003**, *3*, 1375.
(29) Casado, J.; Zgierski, M.; Delgado, M.; Navarrete, J.; Mas-Torrent, M.; Rovira, C. *J. Phys. Chem. C* **2007**, *111*, 10110.
(30) Noda, B.; Wada, H.; Shibata, K.; Yoshino, T.; Katsuhara, M.; Aoyagi1, I.; Taguchi1, T. T.; Kambayashi, T.; Ishikawa, K.; Takezoe, H. *Nanotechnology* **2007**, *18*, 424009.
(31) Schmickler, W.; Widrig, C. *J. Electroanal. Chem.* **1992**, *336*, 213.
(32) Mazur, U.; Hipps, K. W. *J. Phys. Chem. B* **1999**, *103*, 9721.

JP9107427